arXiv:1104.3864v2 [astro-ph.GA] 18 Jul 2011

DISCOVERY OF A CANDIDATE QUIESCENT LOW-MASS X-RAY BINARY IN THE GLOBULAR CLUSTER NGC 6553

Sebastien Guillot[*], Robert E. Rutledge
Department of Physics, McGill University,
3600 rue University, Montreal, QC, Canada, H3A-2T8

Edward F. Brown
Department of Physics and Astronomy, Michigan State University, 3250 Biomedical Physical Science Building, East Lansing, MI
48824-2320, USA

George G. Pavlov
Pennsylvania State University, 512 Davey Lab, University Park, PA 16802, USA and
St.-Petersburg State Polytechnical University, Polytechnicheskaya ul. 29, St.-Petersburg 195251, Russia

Vyacheslav E. Zavlin
Space Science Laboratory, Universities Space Research Association, NASA MSFC VP62, Huntsville, AL 35805, USA
Draft submitted to ApJL on January 20, 2013

ABSTRACT

This paper reports the search for quiescent low-mass X-ray binaries (qLMXBs) in the globular cluster (GC) NGC 6553 using an *XMM-Newton* observation designed specifically for that purpose. We spectrally identify one candidate qLMXB in the core of the cluster, based on the consistency of the spectrum with a neutron star H-atmosphere model at the distance of NGC 6553. Specifically, the best-fit radius found using the three *XMM* European Photon Imaging Camera spectra is $R_{\rm NS} = 6.3^{+2.3}_{-0.8}$ km (for $M_{\rm NS} = 1.4\,M_\odot$) and the best-fit temperature is $kT_{\rm eff} = 136^{+21}_{-34}$ eV. Both physical parameters are in accordance with typical values of previously identified qLMXBs in GC and in the field, i.e., $R_{\rm NS} \sim 5\text{--}20$ km and $kT_{\rm eff} \sim 50\text{--}150$ eV. A power-law (PL) component with a photon index $\Gamma = 2.1^{+0.5}_{-0.8}$ is also required for the spectral fit and contributes $\sim 33\%$ of the total flux of the X-ray source. A detailed analysis supports the hypothesis that the PL component originates from nearby sources in the core, unresolved with *XMM*. The analysis of an archived *Chandra* observation provides marginal additional support to the stated hypothesis. Finally, a catalog of all the sources detected within the *XMM* field of view is presented here.

Subject headings: stars: neutron — X-rays: binaries — globular clusters: individual (NGC 6553)

1. INTRODUCTION

The faint X-ray emission ($L_{\rm X} \sim 10^{32}\text{--}10^{33}\,{\rm erg\,s^{-1}}$) of transiently accreting low-mass X-ray binaries in quiescent state (qLMXBs) was historically interpreted as a thermal blackbody with emission area smaller than that expected for a 10 km neutron star (NS). It was later claimed that the observed luminosity was not due to low accretion rate onto the NS surface, as initially suggested (van Paradijs et al. 1987), but due to heat from the NS crust radiating through the upper layers of the NS atmosphere (Brown et al. 1998). In this interpretation, called Deep Crustal Heating, the energy is deposited in the NS crust by pressure-sensitive nuclear reactions (electron captures, neutron emissions and pycnonuclear reactions, Gupta et al. 2007; Haensel & Zdunik 2008), as matter accumulates on the surface during episodes of rapid accretion. This chain of reactions, from the NS surface to depths with the density of undifferentiated equilibrium, releases $\sim 1.5\,{\rm MeV}$ per accreted nucleon in the crust. In a steady state, these reactions give rise to a time-averaged luminosity, which is directly proportional to the time-averaged mass accretion rate (Brown et al. 1998):

$$\langle L \rangle = 9\times10^{32}\,\frac{\langle \dot{M} \rangle}{10^{-11}\,M_\odot\,{\rm yr^{-1}}}\,\frac{Q}{1.5\,{\rm MeV/amu}}\,{\rm erg\,s^{-1}} \tag{1}$$

where Q is the average heat deposited in the NS crust per accreted nucleon.

The resulting thermal spectrum is described by a realistic NS atmosphere composed exclusively of hydrogen. Indeed, the gravitational settling of the accreted material from the low-mass companion star happens on time scales of $\sim$seconds (Bildsten et al. 1992), resulting in a pure H-atmosphere around the NS. The current models of NS H-atmosphere (Zavlin et al. 1996; McClintock et al. 2004; Heinke et al. 2006a) show that the observed emission is consistent with that from the entire surface area of a $\sim$10 km NS (Rutledge et al. 1999). The H-atmosphere interpretation allows observers to determine the physical radius $R_{\rm NS}$ (or the projected radius $R_\infty = R_{\rm NS}(1+z)$, with $1 + z = \left(1 - 2GM_{\rm NS}/R_{\rm NS}c^2\right)^{-1/2}$) using spectral fitting in the

[*]Vanier Canada Graduate Scholar
Electronic address: guillots@physics.mcgill.ca

soft X-ray range, where the thermal spectrum of qLMXBs peaks.

The radius measurement of NSs using the thermal spectrum of qLMXBs is one way to place constraints on the equation of state (EoS) of dense nuclear matter. This relation between the pressure and the density in the interior of NSs is highly uncertain and multiple competing theories are proposed to explain the behavior of cold matter at densities above $2.35 \times 10^{14} \, \mathrm{g \, cm^{-3}}$. Quiescent LMXBs found in globular clusters (GCs) are routinely used to produce precise measurements of NS radii. The distance to GCs are generally known with precisions of the order of $\sim 5\%$–10% and the overabundances of NS binary systems in GCs (Hut et al. 1992) make these objects ideal targets to pursue searches of qLMXBs capable of providing useful constraints on the dense matter EoS.

Twenty-six GC qLMXBs, including the more recent candidates, have been discovered so far (see Heinke et al. 2003a; Guillot et al. 2009a, for complementary lists). However, for some of them, the poorly constrained R_{NS} and kT_{eff} measurements, as well as the high galactic absorption in their direction (for example, $N_{\mathrm{H}} \sim 1.2 \times 10^{22} \, \mathrm{atoms \, cm^{-2}}$ in the direction of Terzan 5), affects the certainty of their identification. While qLMXBs in the field of the Galaxy or in GC have been observed in quiescence following outbursts events in historical X-ray transients, none of the spectrally identified qLMXBs in GC (with spectra consistent with NS atmosphere models or via their X-ray spectral colors) have been observed in outbursts. There has been one exception recently discovered. An X-ray transient in the cluster Terzan 5 has been observed in outburst (Bordas et al. 2010; Pooley et al. 2010; Degenaar & Wijnands 2011) after being tentatively classified as a qLMXB (CX25, Heinke et al. 2006b). To increase the list of known GC qLMXBs, a program of short observations using the European Photon Imaging Cameras (EPIC; Strüder et al. 2001) onboard *XMM-Newton* have been undertaken to survey GCs and search for qLMXBs. This paper reports the discovery via spectral identification of a candidate qLMXB in the core of NGC 6553. A short archived *Chandra* observation targeted at this GC was also analyzed to provide more accurate positions and tentatively confirm the source classification.

The targeted cluster, NGC 6553, is a low-galactic latitude GC located at the position R.A.$=18^{\mathrm{h}}09^{\mathrm{m}}17.6^{\mathrm{s}}$ and decl. $= -25°54'31''.3$ (J2000), approximately 2.2 kpc from the galactic center, corresponding to a heliocentric distance of $d = 6.0$ kpc. It is a GC of moderate core compactness and moderate size: core radius $r_c = 0'.55$, half mass radius $r_{\mathrm{HM}} = 1'.55$ and tidal radius $r_t = 8'.16$. Its metallicity [M/H] $= -0.09$ (Valenti et al. 2007) makes it one of the most metallic clusters in the Galaxy. The foreground reddening $E(B-V) = 0.63$ corresponds to a moderately high hydrogen column density $N_{\mathrm{H}} = 0.35 \times 10^{22} \, \mathrm{atoms \, cm^{-2}}$ (Predehl & Schmitt 1995). The hydrogen column density is written $N_{\mathrm{H},22} = 0.35$ afterward, and this value will be used for the X-ray spectral fits. This value is similar to the value found from NRAO data (Dickey & Lockman 1990) [1], which accounts for the atomic hydrogen N_{HI} through the entire galaxy. The GC properties come from the catalog of GCs (Harris

1996, update Dec. 2010), except when other references are provided.

The organization of this paper is as follows. Section 2 describes the data reduction and analysis of the *XMM-Newton* and *Chandra* observations. In Section 3, we present the results and we discuss them and conclude in Section 4

2. DATA REDUCTION AND ANALYSIS

NGC 6553 was observed with *XMM-Newton* on 2006 October 6 at 01:41:44 UT, using the three EPIC cameras, for an exposure time of 20.4 ks, with the medium filter. The *Chandra X-ray Observatory* observed the GC for 5.25 ks, on 2008 October 30 at 01:38:12 UT, with the ACIS-S detector (Garmire et al. 2003) in VERY-FAINT mode.

2.1. *Data reduction*

Reduction of *XMM-Newton* data is performed with the *XMM-Newton* Science Analysis Software (SAS) v8.0.0, using the standard procedures[2]. More specifically, `epchain` and `emchain` are used for the preliminary reduction of the raw pn and MOS data files, respectively. Single and double patterns are used for pn data and single, double and quadruple patterns for the MOS cameras, both in the 0.3–10 keV range. Prior to the source detection, the data are checked for background flares by looking for $> 3\sigma$ deviation from the mean count rate of the entire detector. None are found and the whole integration time is used. Also, an exposure map is created to correct for the effect of vignetting. The script `wavdetect` from CIAO v4.2 (Fruscione et al. 2006) is then run on the pn image in the 0.3–10 keV range, with the following parameters: minimum relative exposure of 0.1, the wavelet scales *"1.0 2.0 4.0 8.0"* and a significance threshold 3×10^{-6}. The latter is equal to the inverse of the number of pixels in the image, and allows for about one spurious detection in the entire image. Sources with detection significance $\sigma > 4$ are retained for analysis.

The reduction and analysis of the *Chandra* data are accomplished with the CIAO v4.2 package (Fruscione et al. 2006). The level-1 event file is first reprocessed using the public script *chandra_repro* which performs the steps recommended by the data preparation analysis thread[3] (corrections for charge transfer inefficiency, destreaking, bad pixel removal, etc, if needed) making use of the latest effective area maps, quantum efficiency maps, and gain maps of CALDB v4.3 (Graessle et al. 2007). The newly created level-2 event file is then checked for background flares, but there are none detected.

2.2. *Count extraction*

The command `evselect` from the SAS is used for source and background count extraction of the *XMM* data. A radius of $30''$ around each source is chosen, accounting for 88% of the total energy from an on-axis source at 1.5 keV with the pn detector[4]. The background counts, used for background subtraction, are extracted from a larger region ($100''$) around the source of interest,

---

[1] From http://cxc.harvard.edu/toolkit/colden.jsp

[2] User Guide to the *XMM-Newton* Science Analysis System, Issue 5.0, 2008 (ESA: *XMM-Newton* SOC).

[3] http://cxc.harvard.edu/ciao/threads/data.html

[4] From *XMM-Newton* Users Handbook, Figure 3.7, July 2010

excluding the source itself and other detected sources in close proximity with a circular region of $40''$ around each of them, ensuring that 92% of the overlapping source counts (at $1.5\,$keV on the pn detector) are excluded. In some cases, the close proximity of the detected sources requires to adapt the exclusion radii of nearby sources. Those few cases are discussed in Section 3. The tasks `rmfgen` and `arfgen` generate the response matrix files (RMF) and the ancillary response files (ARF) for each observations. The *XMM-Newton* extracted counts are binned using `grppha` into energy bins between 0.3 and $10\,$keV with a minimum of 20 counts per bin. This criterion ensures having approximate Gaussian statistics in each spectral bin.

For *Chandra* data, the script `psextract` is used to extract the counts of the X-ray sources, in the energy range $0.5–8\,$keV. The extraction region depends on the off-axis angle since the point spread function (PSF) degrades at large off-axis angles. Since the analyzed observation of NGC 6553 was performed with the ACIS-S instrument and a focal plane temperature of $-120\,°$C, the RMFs have to be recalculated, according to the recommendations of the CIAO Science Thread *"Creating ACIS RMFs with mkacisrmf"*. It is also crucial to recalculate the ARFs using the new RMFs in order to match the energy grids between the two files.

In both the *XMM-Newton* and *Chandra* observations, the count rates are low enough for the effects of pile-up to be ignored. Specifically, for the *Chandra* data, the count rate was 0.031 photons per detector frame (3.24 sec), and therefore the effect of pile-up can be safely neglected.

2.3. *Spectral Analysis*

The identification of candidate qLMXBs in this analysis is based on the spectral identification with the models that empirically describe the spectra of previously known qLMXBs. Spectra from the pn camera are first extracted and analyzed, since its superior efficiency facilitates spectral analysis with an improved signal-to-noise ratio (S/N) over the two MOS cameras. H-atmosphere models are available in *XSPEC* (Arnaud 1996), including `nsa` and `nsagrav` (Zavlin et al. 1996) and `nsatmos` (McClintock et al. 2004; Heinke et al. 2006a). The major difference between the models resides in the surface gravity values g used to calculate the model: `nsa` has been implemented with a fixed value $g = 2.43 \times 10^{14}\,$cm s^{-2}, `nsagrav` has been computed for a range $g = (0.1–10) \times 10^{14}\,$cm s^{-2} and `nsatmos` for the range $g = (0.63–6.3) \times 10^{14}\,$cm s^{-2}. Previous works have demonstrated that NS atmosphere models calculated with multiple values of g are better adapted to fit the thermal spectra of qLMXBs (Heinke et al. 2006a; Webb & Barret 2007). We choose here to use `nsatmos`.

The identification of candidate qLMXBs is based on the statistical consistency (null hypothesis probability n.h.p $\gtrsim 10^{-2}$) with the `nsatmos` model at the distance of the host GC, with the galactic absorption taken into account using the multiplicative model `wabs`. Additional conditions impose that the best-fit effective temperature and projected radius are within the range of previously observed GC qLMXBs, i.e., $kT_{\rm eff} \sim 50–180\,$eV and $R_\infty \sim 5–20\,$km (see Heinke et al. 2003b; Guillot et al. 2009a, for complementary lists of GC qLMXBs). For

identified candidate qLMXBs, the pn, MOS1 and MOS2 extracted spectra are then fit simultaneously to improve statistics and diminish the uncertainties on the best-fit parameters.

In some cases, an excess of counts at high energy is modeled with an additional power-law (PL) component. This is empirically justified by the fact that qLMXBs sometimes display a hard PL which dominates the spectrum above $2\,$keV. Most qLMXBs in the field of the galaxy have spectra best fitted with H-atmosphere models combined with a hard-photon PL (for example, Cen X-4, Asai et al. 1996; Rutledge et al. 2001b, Aql X-1, Asai et al. 1998; Campana et al. 1998; Rutledge et al. 2001a). It has been claimed that some GC qLMXBs also displayed significant PL contributions (between $\sim 10\%$ and $\sim 50\%$ of the total flux), for example, in NGC 6440 (Cackett et al. 2005), and in Ter 5 (Heinke et al. 2006b). Proposed interpretations of the observed PL tail include residual accretion onto the NS magnetosphere (Grindlay et al. 2001; Cackett et al. 2005), shock emission via the emergence of a magnetic field (Campana & Stella 2000), or an intrabinary shock between the winds from the NS and its companion star (Campana et al. 2004). However, analyses of the quiescent emission of LMXBs have shown evidence of the presence of a variable low-level accretion on the NS; for the LMXB Aql X-1 (Rutledge et al. 2002), for XTE J1701$-$462, (Fridriksson et al. 2010), and for the LMXB Cen X-4 (Cackett et al. 2010).

Such an additional spectral component for qLMXBs in the core of GCs might not necessarily originate from one of the interpretations listed above. For example, a PL component was required in addition to the H-atmosphere model for the spectral fit of the candidate qLMXB XMMU J171433$-$292747 in NGC 6304 observed with *XMM* (Guillot et al. 2009a). However, a short $5\,$ks archived *Chandra* observation demonstrated that the high energy excess of counts noticed for this source originated from another close by X-ray source (possibly a cataclysmic variable) unresolved in the *XMM* data (Guillot et al. 2009b). Then, a longer $100\,$ks *Chandra* exposure confirmed the NS radius measurement and the initially reported results (S. Guillot et al. 2011, in preparation).

The main focus of this paper is the discovery of candidate qLMXBs in NGC 6553, but as part of the systematic analysis of *XMM* data, a simple spectral analysis is performed for all other X-ray sources that are not consistent with NS H-atmosphere models at the distance of the host GC. Specifically, a simple absorbed PL model is used and their best-fit photon indices, as well as their unabsorbed flux ($0.5–10\,$keV) are reported. In some cases, the X-ray spectra cannot be fit adequately with either an NS H-atmosphere model or a PL model. In those cases, the use of other models is attempted for completeness and the details are provided in Section 3. Finally, sources with an $S/N < 3$ are fit with a fixed ($\Gamma = 1.5$) photon index.

In all cases, the galactic absorption is taken into account with the model `wabs`, keeping the value of $N_{\rm H}$ fixed at the value in the direction of the GC, i.e., $N_{\rm H,22} = 0.35$. Also, all quoted uncertainties on the spectral parameters are 90% confidence level in the text and the tables. Finally, the quoted fluxes are corrected for the finite aper-
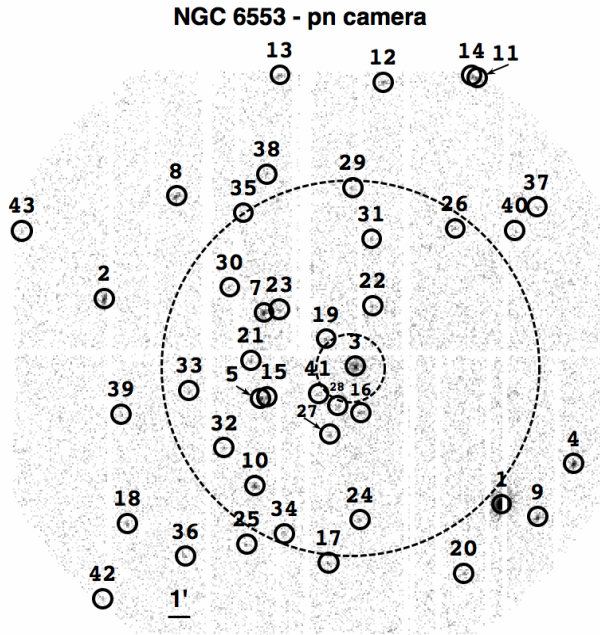
NGC 6553 - pn camera

FIG. 1.— This EPIC/pn image of NGC 6553 shows the 43 sources detected on the pn camera. The small and large dashed circles respectively represent the half-mass ($r_{HM} = 1\!'\!55$) and tidal radii ($r_t = 8\!'\!16$). A log gray-scale has been used for the image due to the brightness of source #1. In this figure, north is up and R.A. increases to the left. The candidate qLMXB detected in this GC is the source #3, corresponding to XMMU J180916−255425.

ture (extraction radius), except noted otherwise.

2.4. *Astrometric correction*

The uncertainties reported in Table 1 on the *XMM* positions are composed of the `wavdetect` statistical error on the pn positions (up to $1''$) and the systematic uncertainty of *XMM* ($2''$at 1σ[5]). An absolute astrometric correction – into the frame of the Two Micron All Sky Survey (2MASS) – is applied through the association of X-ray sources with 2MASS counterparts. Three X-ray sources were firmly associated with 2MASS objects. The sources #5, #2 and #9 have probabilities 0.001%, 0.21% and 0.04%, respectively, that a star as bright or brighter as the stars 2MASS J18093564−25555377, 2MASS J18100723−25511760 and 2MASS J18083961−2601203, respectively, lie as close or closer to the three X-ray sources. These probabilities were calculated using all 2MASS stars detected in $2'$ wide annulli, centered at the GC optical center, and with respective average radii equal to the distances of the respective 2MASS counterparts from the GC center. This means that sources #5, #2 and #9 have probabilities 99.999%, 99.79% and 99.96% to be associated with the stars 2MASS J18093564−25555377, 2MASS J18100723−25511760 and 2MASS J18083961−2601203, respectively. From these three associations, the best-fit required transformation is a shift of -$0\!''\!1$ in R.A. and $0\!''\!71$ in decl. The residual uncertainties are $0\!''\!34$ in R.A. and $1\!''\!08$ in decl. This is added in quadrature to the 2MASS astrometric

uncertainty ($\sim 0\!''\!15$ [6]) and to the statistical uncertainty of the X-ray source detection.

3. RESULTS

In the reduced image of NGC 6553, the `wavdetect` algorithm detected 43 X-ray sources on the pn camera within the field of the observation. Table 1 lists all the sources detected with their positions, their statistical uncertainty and their detection significance, while Table 2 provides the results of the spectral fits and the fluxes. The spectral analysis of candidate qLMXBs and of the sources for which a PL model does not describe the data is detailed below.

As can be seen in Figure 1, the proximity ($17\!''\!5$) of source #15 to source #5 requires to adapt the extraction radius prior to the spectral analysis. More specifically, instead of excluding the default $40''$ around nearby sources, the exclusion radii of source #15 is chosen to be $10''$ (59% of encircled count fraction, ECF) for the count extraction of #5, and the exclusion radii of source #5 is chosen to be $12\!''\!5$ (68% of ECF) for the count extraction of source #15. The radii mentioned were determined by visual inspection of the X-ray image. Similarly, the `wavdetect` algorithm detected two sources, #11 and #14, located $16''$ apart near the edge of the pn camera. In this case, the exclusion radii of #11 and #14 are set to $15''$ and $10\!''\!5$, when considering the extraction region of sources #14 and #11, respectively.

3.1. *Source #1 - XMMU J180846−260043*

This X-ray source has the largest pn count rate of the observation, $0.197 \pm 0.004\,\mathrm{cts\,s^{-1}}$. Nevertheless, it is not affected pile-up (accumulation of photon events within a single CCD time frame, $73\,\mathrm{ms}$) since its count rate per detector frame is then ~ 0.014.

The bright X-ray source corresponds to the *ROSAT* source 1RXS J180847.7-260037 (Voges et al. 1999) and to the IR star 2MASS J18084678-2600417 (with probability of association 99.999%). It is also named, HD 315209, as listed in the Tycho Reference Catalog with the proper motion $+14.2 \pm 2.4\,\mathrm{mas\,yr^{-1}}$ in R.A. and $-9.0 \pm 1.7\,\mathrm{mas\,yr^{-1}}$ in decl. (Høg et al. 1998, 2000). The star has a spectral type K5V and is located at a distance of $33\,\mathrm{pc}$, deduced from spectroscopic observations (Riaz et al. 2006).

The *XMM* source is adjacent to a bad column on the pn camera. Therefore, the resulting astrometry is likely to be offset in the direction opposite to the bad column, i.e., toward increasing right ascension. Therefore, we provide the position obtained with the MOS2 camera – R.A.=$18^h08^m46.7^s$ and decl. = $-26°00'42\!''\!7$.

The high-S/N spectrum of this star is not well described by an absorbed PL: χ^2_ν/dof (prob.) = $1.80/120$ (1.7×10^{-7}). Removing the absorption, i.e., setting N_H=0, also leads to a non-acceptable fit with n.h.p. $\sim 10^{-60}$. Similarly, NS H-atmosphere, thermal bremsstrahlung and blackbody models do not fit properly the data, leading to n.h.p. $< 10^{-10}$, whether or not galactic absorption is included with the models fitted. A Raymond-Smith (RS) plasma model provides improved fit statistics with n.h.p. $\approx 10^{-3}$ but

TABLE 1
X-RAY SOURCES DETECTED IN THE *XMM* OBSERVATION OF NGC 6553.

Object Name	RA (J2000)	decl. (J2000)	$\delta_{\mathrm{R.A.}}\backslash\delta_{\mathrm{decl.}}$ [a] ($''$)	S/N [b]	ID
XMMU J180846−260043	272.19551	-26.01220	±0.0\0.0	166.1	01
XMMU J181007−255118	272.53028	-25.85518	±0.3\0.3	28.0	02
XMMU J180916−255425	272.31889	-25.90704	±0.4\0.3	26.2	03
XMMU J180832−255852	272.13472	-25.98135	±0.4\0.4	24.6	04
XMMU J180935−255554	272.39844	-25.93172	±0.4\0.5	22.6	05
XMMU J180845−260035	272.18903	-26.00978	±0.4\0.4	21.4	06
XMMU J180935−255157	272.39592	-25.86605	±0.3\0.3	21.3	07
XMMU J180952−254637	272.46964	-25.77697	±0.7\0.6	16.9	08
XMMU J180839−260118	272.16497	-26.02191	±0.6\0.5	16.7	09
XMMU J180936−255952	272.40357	-25.99803	±0.6\0.5	15.5	10
XMMU J180851−254113	272.21633	-25.68706	±0.6\0.5	14.1	11
XMMU J180910−254125	272.29530	-25.69036	±0.5\0.5	12.1	12
XMMU J180931−254105	272.38234	-25.68474	±0.6\0.4	10.9	13
XMMU J180853−254106	272.22092	-25.68513	±0.6\0.5	9.3	14
XMMU J180934−255549	272.39324	-25.93030	±0.5\0.4	9.2	15
XMMU J180915−255631	272.31424	-25.94212	±0.7\0.5	9.0	16
XMMU J180921−260325	272.34126	-26.05712	±1.0\0.7	8.0	17
XMMU J181002−260135	272.51131	-26.02663	±0.6\0.7	7.9	18
XMMU J180922−255310	272.34343	-25.88638	±0.9\0.6	7.5	19
XMMU J180854−260353	272.22729	-26.06497	±0.6\0.5	7.4	20
XMMU J180937−255408	272.40664	-25.90245	±0.5\0.5	7.3	21
XMMU J180912−255138	272.30407	-25.86082	±0.8\0.8	6.6	22
XMMU J180931−255149	272.38286	-25.86367	±0.8\0.6	6.4	23
XMMU J180915−260127	272.31512	-26.02427	±0.9\0.9	6.3	24
XMMU J180938−260233	272.41026	-26.04259	±1.0\0.6	6.2	25
XMMU J180856−254806	272.23482	-25.80185	±0.9\0.7	6.2	26
XMMU J180921−255731	272.34030	-25.95878	±0.8\0.7	6.2	27
XMMU J180920−255614	272.33388	-25.93725	±0.7\0.6	5.9	28
XMMU J180917−254614	272.32096	-25.77083	±0.9\0.7	5.8	29
XMMU J180941−255048	272.42476	-25.84671	±0.9\0.8	5.7	30
XMMU J180913−254834	272.30522	-25.80972	±0.9\0.8	5.6	31
XMMU J180943−255808	272.42940	-25.96905	±0.7\0.7	5.6	32
XMMU J180950−255531	272.45886	-25.92548	±0.7\0.6	5.5	33
XMMU J180930−260205	272.37870	-26.03489	±0.8\0.8	5.5	34
XMMU J180939−254723	272.41319	-25.78992	±0.0\0.0	5.4	35
XMMU J180950−260307	272.46218	-26.05219	±0.9\0.7	5.4	36
XMMU J180839−254707	272.16615	-25.78536	±0.7\0.6	5.3	37
XMMU J180934−254537	272.39339	-25.76053	±0.6\0.6	5.2	38
XMMU J181003−255636	272.51627	-25.94347	±0.7\0.6	5.0	39
XMMU J180844−254812	272.18444	-25.80336	±0.8\0.7	4.6	40
XMMU J180924−255540	272.35017	-25.92790	±0.7\0.6	4.5	41
XMMU J181007−260503	272.53191	-26.08422	±0.7\1.0	4.4	42
XMMU J181023−254811	272.59968	-25.80325	±0.7\0.7	4.2	43

[a] Statistical uncertainty on the position
[b] Detection significance provided by `wavdetect`

this is still not a statistically acceptable fit. A two-temperature RS model, often used to represent stellar coronal spectra (Dempsey et al. 1993), satisfactorily describes the spectrum, χ^2_ν/dof (prob.) = 1.01/11.5 (0.44), with best-fit temperatures $kT_{\mathrm{eff},1} = 0.35^{+0.05}_{-0.12}$ keV and $kT_{\mathrm{eff},2} = 2.80^{+5.75}_{-0.67}$ keV. With this model, the best-fit hydrogen column density is $N_{\mathrm{H},22} = 0.09 \pm 0.04$, consistent with a small distance to this star which lies in the foreground of NGC 6553.

3.2. *Source #5 - XMMU J180935−255554*

This source, located within the GC tidal radius, is likely associated with the star HD 165973 of spectral type G8III (Houk & Smith-Moore 1988). The 2MASS name of this star is 2MASS J18093564-2555537 (99.999% chance of association with the X-ray source #5). It has a proper motion of $+12.9\pm1.9$ mas yr^{-1} in R.A. and -3.5 ± 1.6 mas yr^{-1} in decl. (Høg et al. 1998, 2000). No parallax measurement is available for this star.

The X-ray spectrum cannot be fit with the NS H-atmosphere, PL, blackbody and thermal bremsstrahlung models. All of these models lead to n.h.p. < 0.006. However, an RS plasma model provides a statistically acceptable fit with χ^2_ν/dof (prob.) = 0.75/13 (0.71). The best-fit temperature is $kT_{\mathrm{eff}} = 0.37^{+0.07}_{-0.12}$ keV and the best-fit hydrogen column density is $N_{\mathrm{H},22} < 0.26$ (90% confidence upper limit).

3.3. *Source #9 - XMMU J180839−260118*

The source #9 has a soft thermal spectrum that is found to be acceptably fit by the `nsatmos` model: $kT_{\mathrm{eff}} = 80^{+21}_{-12}$ eV and $R_{\mathrm{NS}} = 15.4^{+6.3}_{-6.0}$ km for $M_{\mathrm{NS}} = 1.4\,M_\odot$, with χ^2_ν/dof (prob.) = 1.50/32 (0.03). The spectrum is also acceptably fit with a RS plasma model: $kT_{\mathrm{eff}} = 0.87^{+0.15}_{-0.09}$ keV, $N_{\mathrm{H},22} = 0.19^{+0.07}_{-0.08}$ and $Z = 0.10^{+0.16}_{-0.06}$ with χ^2_ν/dof (prob.) = 1.20/30 (0.21). A Kolmogorov-Smirnov test (probability $p = 0.22$) shows no evidence of variability.

TABLE 2
Spectral results of X-ray sources in NGC 6553.

ID	pn Rate (cts ks^{-1})	Γ	kT_{eff} (keV)	F_{X}	χ^2_ν/d.o.f. (prob.)	Model Used
01	197.3±3.8	–	$0.35^{+0.05}_{-0.12}$; $2.80^{+5.75}_{-0.67}$	17.3	1.01/115 (0.44)	RS+RS
02	17.7±1.3	$3.0^{+0.3}_{-0.3}$	–	2.54	1.32/15 (0.18)	PL
03	27.1±1.5 ^{a}	$2.1^{+0.5}_{-0.8}$	$0.136^{+0.021}_{-0.034}$	1.29	0.90/54 (0.68)	NSATMOS+PL
04	18.1±1.4	$1.4^{+0.2}_{-0.2}$	–	2.67	0.79/18 (0.71)	PL
05	15.0±1.3	–	$0.37^{+0.07}_{-0.12}$	0.42	0.75/13 (0.71)	RS
06	8.6±0.9	$3.3^{+0.5}_{-0.4}$	–	5.89	1.50/ 7 (0.16)	PL
07	17.6±1.4	$0.9^{+0.2}_{-0.2}$	–	2.46	0.75/18 (0.76)	PL
08	10.8±1.1	$0.8^{+0.3}_{-0.3}$	–	2.72	0.94/11 (0.50)	PL
09	11.6±1.2	–	$0.873^{+0.145}_{-0.092}$	0.65	1.20/30 (0.21)	RS
10	9.6±1.1	$2.4^{+0.5}_{-0.4}$	–	0.74	0.75/12 (0.70)	PL
11	6.0±0.9	$0.7^{+0.3}_{-0.4}$	–	2.58	0.85/ 6(0.53)	PL
12	4.0±1.0	$-0.3^{+0.7}_{-0.7}$	–	2.44	0.83/ 8 (0.58)	PL
13	3.9±0.9	$1.2^{+0.6}_{-0.6}$	–	1.07	0.92/ 6 (0.48)	PL
14	3.7±0.7	$0.2^{+0.6}_{-0.7}$	–	2.2	0.66/ 3 (0.57)	PL
15	6.7±1.0	$2.8^{+0.8}_{-0.8}$	–	0.44	2.02/ 8 (0.04)	PL
16	4.5±1.0	$4.5^{+1.5}_{-1.3}$	–	0.31	1.27/ 9 (0.25)	PL
17	4.3±0.9	$3.9^{+1.2}_{-1.1}$	–	0.34	2.15/ 7 (0.03)	PL
18	5.1±1.0	$1.5^{+0.5}_{-0.5}$	–	0.96	0.59/ 8 (0.79)	PL
19	3.7±1.0	$1.3^{+0.7}_{-0.7}$	–	0.30	0.86/ 9 (0.56)	PL
20	4.0±0.9	$5.0^{+1.4}_{-1.2}$	–	0.51	1.30/ 7 (0.25)	PL
21	4.4±0.9	$3.5^{+1.0}_{-0.9}$	–	0.31	1.14/ 7 (0.33)	PL
22	2.3±0.9	(1.5)	–	0.13	0.54/ 8 (0.82)	PL
23	4.6±1.0	$2.1^{+0.7}_{-0.6}$	–	1.60	0.65/ 8 (0.74)	PL
24	3.5±0.9	$1.0^{+0.6}_{-0.6}$	–	0.47	1.31/ 7 (0.24)	PL
25	4.4±0.9	$1.4^{+1.7}_{-1.1}$	–	0.44	1.84/ 7 (0.08)	PL
26	2.6±0.9	$1.4^{+1.2}_{-1.4}$	–	0.28	0.52/ 6 (0.79)	PL
27	1.5±0.9	(1.5)	–	0.08	0.95/ 8 (0.37)	PL
28	0.4±0.9	(1.5)	–	0.05	2.26/ 7 (0.03)	PL
29	3.3±0.8	$0.3^{+0.9}_{-1.0}$	–	0.75	0.34/ 5 (0.89)	PL
30	3.0±0.8	$1.8^{+1.3}_{-0.9}$	–	0.29	0.60/ 5 (0.70)	PL
31	3.0±0.9	$1.4^{+0.9}_{-0.8}$	–	0.30	0.36/ 7 (0.93)	PL
32	1.5±0.9	(1.5)	–	0.20	0.39/ 7 (0.91)	PL
33	2.2±0.9	(1.5)	–	0.21	0.47/ 7 (0.86)	PL
34	2.7±0.8	$1.6^{+1.2}_{-1.1}$	–	0.31	0.56/ 5 (0.73)	PL
35	4.1±0.8	$3.8^{+0.7}_{-0.7}$	–	0.51	0.63/ 8 (0.85)	PL
36	3.8±0.9	$2.8^{+0.7}_{-0.7}$	–	0.45	1.66/ 7 (0.11)	PL
37	2.0±0.8	(1.5)	–	0.09	2.25/ 6 (0.04)	PL
38	3.3±0.9	$3.9^{+2.1}_{-2.0}$	–	0.33	1.07/ 6 (0.38)	PL
39	3.0±0.9	$4.3^{+3.4}_{-2.2}$	–	0.33	0.63/ 6 (0.70)	PL
40	1.7±0.8	(1.5)	–	0.20	0.66/ 5 (0.65)	PL
41	0.7±0.9	(1.5)	–	0.01	2.01/ 7 (0.05)	PL
42	0.4±0.7	(1.5)	–	0.24	1.37/ 4 (0.24)	PL
43	1.8±0.8	(1.5)	–	0.49	0.88/ 5 (0.50)	PL

NOTE. — The columns of this table are, from left to right: the source ID according to Table 1, the background subtracted count rates in the 0.3–10 keV range, the best-fit photon index when a `power law` was used (values in parentheses were held fixed), the best-fit effective temperature when a thermal model was used, and the unabsorbed X-ray flux in unit of 10^{-13} erg cm^{-2} s^{-1} in the band 0.5–10 keV. Note that the flux is not corrected for the finite aperture in this table. This energy range is different from that used for the spectrum extraction (0.3–10 keV), for comparison purposes with previously published work. The last column is the resulting χ^2-statistic and the model used (PL: power law, RS: Raymond-Smith plasma). All fits have been performed with a fixed value of the galactic absorption, $N_{\text{H},22}$=0.35.

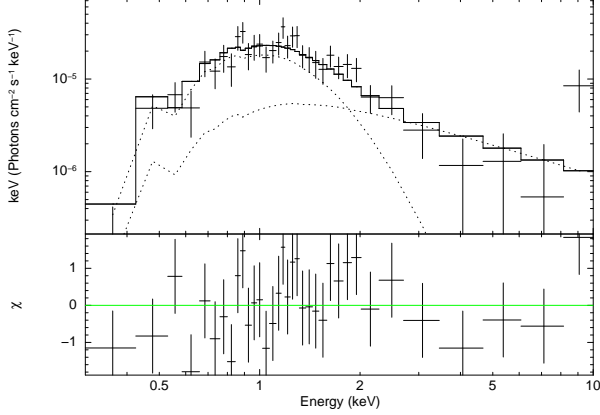^{a} The MOS1/2 count rates are respectively 8.5±0.8 and 6.6±0.7 counts per ksec in the 0.3-10 keV range.

FIG. 2.— *XMM*-pn spectrum of the candidate qLMXB XMMU J180916−255425 in NGC 6553. The two components (H-atmosphere `nsatmos` and PL `powerlaw`) are shown in dashed lines. They are both affected by interstellar absorption modeled with `wabs` and the hydrogen column density $N_{\rm H,22}$=0.35. The PL dominates the spectrum at $E \gtrsim 2\,{\rm keV}$.

The infrared (IR) source, 2MASS J18083961−2601203, is located at a distance of $1''51$ from source #9 (after correction) and is identified as the probable counterpart of the candidate qLMXB, with a probability of association of 99.86%. It has magnitudes in the J, H and K IR bands of $m_J = 10.146\,(15)$, $m_H = 9.796\,(23)$, and $m_K = 9.723\,(31)$, where the numbers in parentheses indicate the uncertainties on the magnitudes. The X-ray to J-band flux ratio of the association is $F_{\rm X}/F_J \approx 2\times10^{-3}$ and is consistent with that of a coronally active star. The possibility that source #9 is a qLMXB with a giant star in NGC 6553 cannot be discarded on this basis.

However, in the color-magnitude diagram of NGC 6553 (Ortolani et al. 1995), the V-band magnitude of this star in the NOMAD Catalogue (Zacharias et al. 2005) lies ∼ 5 mag above the tip of the red giant branch. This observation strongly disfavors the giant star hypothesis, since the star is ∼ 100× brighter than the brightest giants in the cluster. In addition, the location of the system outside the tidal radius of the cluster also disfavors the qLMXB classification. Therefore, we conclude that source #9 is not a candidate qLMXB at the distance of the GC.

3.4. Candidate qLMXB, source #3 - XMMU J180916−255425

3.4.1. XMM-Newton observation

The X-ray spectrum of this source is acceptably fit (χ^2_ν/dof (prob.) = 1.44/33 (0.05)) with `nsatmos`, for which the parameters are: $R_{\rm NS} = 6.7^{+0.9}_{-1.2}\,{\rm km}$ and $kT_{\rm eff} = 137^{+20}_{-18}\,{\rm eV}$, for $M_{\rm NS} = 1.4\,M_\odot$. However, an additional PL component is required to account for the high-energy tail of the spectrum, as evidenced by a low f-test probability (prob.=0.002). Adding the PL component to `nsatmos` results in the following improved fit : χ^2_ν/dof (prob.) = 0.97/31 (0.52), with $R_{\rm NS} = 6.3^{+2.9}_{-1.0}\,{\rm km}$ ($M_{\rm NS} = 1.4\,M_\odot$), $kT_{\rm eff} = 135^{+25}_{-42}\,{\rm eV}$ and $\Gamma = 2.1^{+1.5}_{-0.9}$ (Figure 2). The best-fit projected radius R_∞ and temperature are consistent with the qLMXB classification. There is no evidence of variability on the timescale of the observation as evidenced by a Kolmogorov-Smirnov

test (probability $p = 0.25$).

To improve the statistics, the MOS1 and MOS2 extracted spectra are added in *XSPEC* and a simultaneous spectral fit is performed. A multiplicative constant is added to the `nsatmos + powerlaw` model to verify that there is no discrepancy between the pn spectrum and the MOS1/2 spectra normalizations. The multiplicative constant is fixed to $c = 1$ for pn and fit for the MOS1/2 data. It is found that $c_{\rm MOS1} = 1.08^{+0.20}_{-0.18}$ and $c_{\rm MOS2} = 0.86^{+0.17}_{-0.16}$, both consistent with unity. Consequently, no discrepancy is observed and the simultaneous fit is performed with the values fixed at $c = 1$ for all three spectra. The best-fit `nsatmos + powerlaw` parameters are listed in Table 3. The NS parameters and the unabsorbed luminosity (thermal component $L_{\rm X,th} = 4.2\times10^{32}\,{\rm erg\,s^{-1}}$, and PL component $L_{\rm X,PL} = 2.1\times10^{32}\,{\rm erg\,s^{-1}}$, in the 0.5–10 keV range) are within the expected range of values for qLMXBs.

The PL component accounts for 33% of the total unabsorbed flux. Such a strong PL component, if not intrinsic to the source, could suggest that, as observed for the candidate qLMXB in the core of NGC 6304 (Guillot et al. 2009b), multiple X-ray sources are unresolved in the core. Running the detection algorithm `wavdetect` on the MOS1/2 images (because of the smaller pixel size than the pn camera) does not reveal the presence of multiple resolved sources in the core. Nonetheless, visual inspection of the EPIC images seems to suggest that the spatial count distribution deviates from that of a point source, favoring the hypothesis that nearby sources are unresolved by *XMM-Newton*.

A more quantitative analysis is performed using the *XMMSAS* task `eradial`. By comparing the spatial distribution of counts to the telescope PSF (Figure 3), there is marginal evidence that the source differs from a point source (χ^2=51.5 for 31 degrees of freedom (dof), with n.h.p = 1.2%). In other words, there is marginal support to the hypothesis that the qLMXB candidate is confused with nearby sources (at ∼ $15''$–$30''$) in the *XMM* data. For this fit and for Figure 3, the radial extent of the PSF is cut off at $100''$, the distance of the next closest X-ray source detected. However, the fit statistics are highly dependent on the radial extent of the PSF. For example, choosing instead a cut off at $30''$ leads to χ^2=30.1 for 9 dof, with n.h.p = 0.04%, which is strong evidence for the presence of nearby unresolved sources.

The hypothesis that the PL component is due to nearby sources is further tested by using a spectrum created from counts located within $12''$ of the source center, therefore decreasing the contamination from possible nearby sources at $> 12''$, as evidenced by the PSF analysis above. However, this method reduces the S/N since only 62% of the ECF is included within $12''$ at 1.5 keV. This spectrum has a count rate of 15±1 cts ks^{-1}. Using the `nsatmos` model alone, the best-fit parameters, $R_{\rm NS} = 6.4^{+1.8}_{-0.8}\,{\rm km}$ (for $M_{\rm NS} = 1.4\,M_\odot$) and $kT_{\rm eff} = 135^{+19}_{-27}\,{\rm eV}$, are consistent with the best-fit parameters mentioned above, as is the unabsorbed flux $F_{\rm X} = 1.49\times10^{-13}\,{\rm erg\,cm^{-2}\,s^{-1}}$. The statistically acceptable fit, χ^2_ν/dof (prob.) = 1.73/12 (0.05), does not require a PL component, as demonstrated by the high F-test probability (prob. = 0.31). Adding a PL component leads to consistent NS parameters and flux. Also, the
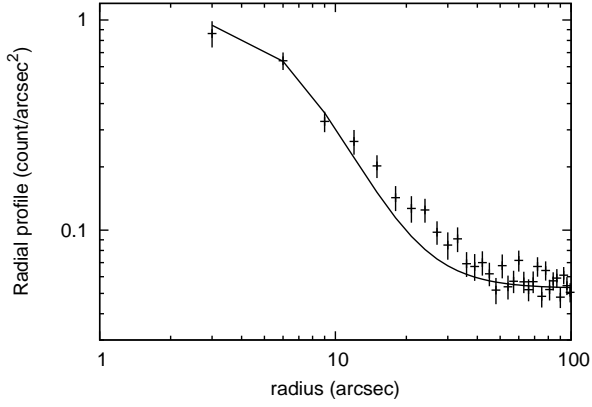
FIG. 3.— *XMM* surface brightness as a function of radius of the candidate qLMXB in the core of NGC 6553. The line indicates the best-fit pn-camera point-spread function at the position of the source. Counts in excess of the telescope PSF at $\sim 15''$–$30''$ are evidence of the presence of one (or more) unresolved sources. This is marginally supported by the statistic of the PSF fit: $\chi^2 = 51.5$ for 31 d.o.f., with n.h.p.=1.2%.

fraction of the PL to the total flux is consistent with zero at the 1σ level. This provides additional support to the claim that the PL component represents the emission of nearby contaminating sources at angular distances $> 12''$ from the qLMXB candidate in the core of NGC 6553.

Finally, the second *XMM-Newton* serendipitous source catalog (2XMMi; Watson et al. 2009) reports two sources located $20''.7$ apart, at the positions R.A.=$18^{\rm h}09^{\rm m}16.5^{\rm s}$ and decl. $= -25°54'26''.1$ for the brightest one, coincident with the qLMXB and, R.A.=$18^{\rm h}09^{\rm m}18.0^{\rm s}$ and a fainter nearby source at decl. $= -25°54'27''.5$. The discrepancy between 2XMMi and the detections in this work may reside in the algorithm used. While we performed the detection with `wavdetect`, the 2XMMi sources are detected with a sliding box algorithm. In addition, we used the pn data only, while the 2XMMi catalog is constructed with a pn+MOS1/2 mosaic.

Overall, the above analysis supports the hypothesis that one or more nearby sources produce the observed PL component. However, only the angular resolution of the *Chandra X-ray Observatory* offers the possibility to ascertain that the above claim is correct, by spatially and spectrally differentiating multiple sources. Archived *Chandra* data of NGC 6553 are analyzed and the results are presented in the following subsection.

3.4.2. Chandra *observations of NGC 6553*

The following pertains solely to the confirmation of the candidate qLMXB and makes use of *Chandra*'s angular resolution to understand the core-source emission. A systematic detection and spectral analysis of all X-ray sources are not reported here.

Only one source is detected with `wavdetect` in the core of the GC, with a background subtracted count number of 46.8 ± 6.9 cts. The position of CXOU 180916.48−255426.58 is consistent with the corrected *XMM* position of the candidate qLMXB. The difference between the *Chandra* and *XMM* positions, $1''.4$, is within the accuracy of the *Chandra* systematic uncertainty ($0''.6$) and the *XMM* residual error after the correction ($1''.1$, see Section 2.4). Therefore, the *Chandra*
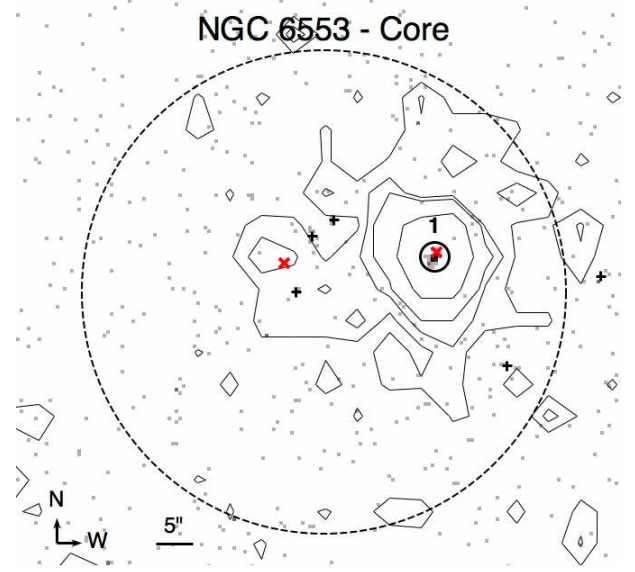

FIG. 4.— *XMM* contours plotted over the *Chandra* ACIS-S3 image. The small circle is the candidate qLMXB detected with *Chandra*. The large dashed circle represents the $0'.55$ core radius of the GC. The red crosses '×' show the positions of the two 2XMMi sources. Finally, the five black '+' signs show the possible sources that have low significance in this short ~ 5 ks *Chandra* observations.

source is consistent with being the same X-ray source as XMMU J180916−255425. Figure 4 shows the *Chandra* image of the GC core, with *XMM* contours and the two 2XMMi catalog sources.

A second possible source, with a 2.1σ significance (1.28 ± 0.54 cts ks^{-1}), lies $17''$ from the core candidate qLMXB, and close ($\sim 5''$) to the faint 2XMMi source. An additional one, ($\sim 4''$) away from the faint 2XMMi source and $19''.5$ distant from the qLMXB candidate, has a significance of 1.6σ. Other faint possible sources, with low-significance (1.6σ, 1.7σ and 2.2σ) are located at distances $14''.8$, $17''.7$ and $22''.7$, respectively (see Figure 4). The extended emission observed in Figure 3 could be explained by the presence of other sources in the GC core. Unfortunately, this short *Chandra* observation does not permit a confident detection of all the sources in the core. Furthermore, restricting counts to the 3–10 keV or the 2–10 keV energy ranges in `wavdetect` does not lead to the detection of any nearby source, suggesting that this excess of counts above 2 keV is not due to a single source, but due to multiple fainter sources. A longer high angular resolution observation of the central region of NGC 6553 would certainly shed light on the PL tail observed in the *XMM* spectrum of the candidate qLMXB

The PL component measured with *XMM* has an absorbed flux $F_{\rm X} = 4.9\times10^{-14}$ erg cm^{-2} s^{-1} in the 0.5–10 keV range with a photon index $\Gamma = 2.1$. Using *webPIMMs*[7], the expected *Chandra*/ACIS-S3 count rate is 4.7 cts ks^{-1} (0.5–8 keV), which corresponds to 23.5 counts on this short *Chandra* observation. However, the *Chandra* background subtracted count rate of an annulus ($r_{\rm in} = 10''$ and $r_{\rm out} = 30''$) centered around the core source is 7 ± 14 cts. The non-detection of an excess of counts around the core source does not support the pos-

---

[7] Available via HEASARC, http://heasarc.gsfc.nasa.gov/Tools/w3pimms.h

TABLE 3
Spectral analysis of the core candidate qLMXB

Detector	Model	$R_{\rm NS}$ (km)	$kT_{\rm eff}$ (eV)	Γ	$F_{\rm X}$	PL Flux (%)	χ^2_ν/d.o.f. (prob.)
EPIC-pn (12″)	NSATMOS + PL	$6.4^{+3.1}_{-1.1}$	131^{+28}_{-42}	$2.0^{+0.8}_{-3.6}$	$1.6^{+6.9}_{-1.2}$	23^{+48}_{-23}	1.37/10 (0.18)
EPIC-pn+MOS1/2	NSATMOS + PL	$6.3^{+2.3}_{-0.8}$	136^{+21}_{-34}	$2.1^{+0.5}_{-0.8}$	$1.5^{+4.2}_{-0.7}$	33^{+32}_{-22}	0.90/54 (0.68)
EPIC+ACIS-S3 [a]	NSATMOS + PL	$6.4^{+2.1}_{-0.8}$	134^{+21}_{-34}	$2.1^{+0.5}_{-0.7}$	$1.5^{+4.3}_{-0.7}$	32^{+35}_{-22}	1.02/58 (0.44)
ACIS-S3	NSATMOS	$6.6^{+3.2}_{-1.3}$	134^{+35}_{-39}	–	$1.0^{+4.6}_{-0.3}$	–	cstat=146.98

NOTE. — In all the fits, the galactic absorption, modeled with wabs, is represented by a fixed value of $N_{\rm H,22} = 0.35$. Γ represents the photon index of the power-law (PL) model. $F_{\rm X}$ is the total unabsorbed flux, in units of $10^{-13}\,{\rm erg\,cm^{-2}\,s^{-1}}$, in the range 0.5–10 keV, with 1σ-errors. PL Flux (%) represents the PL contribution to the total flux (1σ-errors).
[a] For the ACIS-S3 spectrum, the powerlaw normalization is set to zero. The multiplication constant, set free for ACIS-S3, is $c_{\rm ACIS} = 0.85^{+0.43}_{-0.26}$.

sibility that multiple diffuse sources are responsible for the high-energy contamination of the *XMM* spectrum of the candidate qLMXB. This could be explained if the sources are variable.

Alternatively, the detected PL component could be intrinsic to the candidate qLMXB, but display some variability, as has been observed for other LMXBs. This possibility is investigated by extracting counts in the 2–10 keV range. With the pn camera, a count rate of $0.97\pm0.31\,{\rm cts\,ks^{-1}}$ is detected, which corresponds to $0.36\,{\rm cts\,ks^{-1}}$ expected on the ACIS-S3 detector using *webPIMMs*, assuming a photon index $\Gamma = 2.1$. We detect $1.13\pm0.47\,{\rm cts\,ks^{-1}}$ on the *Chandra* data in the 2–10 keV range. These count rates are consistent and therefore there is no observed variability of the high-energy component ($> 2\,{\rm keV}$), at the $< 2\sigma$ level.

The *Chandra* spectrum of the candidate qLMXB in the core of NGC 6553, i.e., image on-axis, is extracted from a 2″.5 radius circular region to include more than 95% of the source energy[8]. For the purpose of the count rate calculation only, the background is extracted using a circular region of 25″ radius around the source , excluding 5″ around the qLMXB itself, which ensures that $> 99\%$ of the ECF is excluded.

Due to the small numbers of counts, a binning of 10 counts per bin is applied for the candidate qLMXB, which only guarantees marginally Gaussian uncertainty in each bin. The binned spectrum is used simultaneously with the three EPIC spectra to evaluate the consistency of the spectra. All parameters are tied between the four spectra. Only the powerlaw norm is set to zero for the *Chandra* observation. Also, a multiplicative constant is added to the model to quantify the variation between EPIC and ACIS-S3 spectra. We find that the best-fit parameters of the four spectra are consistent with that of the EPIC spectra alone (see Table 3 and Figure 5). In addition, the multiplication constant, which was left free for the ACIS-S3 spectrum, is statistically consistent with unity, $c_{\rm ACIS} = 0.85^{+0.43}_{-0.26}$. This is evidence that, within the statistics of the observation, the *Chandra* spectrum is consistent with the three EPIC spectra.

Finally, we also perform a fit of the *Chandra* unbinned spectrum alone, using Cash-statistic (Cash 1979). The background, representing 2.5% of the extracted counts
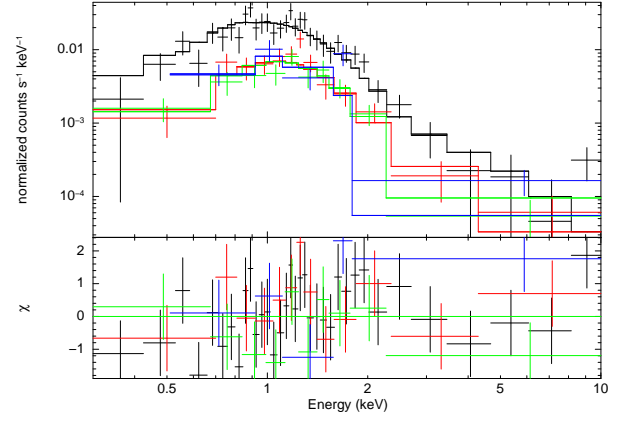
[8] *Chandra* Observatory Proposer Guide, Chap. 6, v11.0, Jan 2009

Fig. 5.— *XMM*-pn (black), MOS1 (red), MOS2 (green) and ACIS-S3 (blue) spectra of the candidate qLMXB of NGC 6553, XMMU J180916−255425, with the best-fit nsatmos+powerlaw model with wabs galactic absorption $N_{\rm H,22}$=0.35. The ACIS-S3 counts are grouped with a minimum of 10 cts per bin, due to the small number of counts. The fit statistic χ^2_ν/dof (prob.) = 1.02/58 (0.44) and the multiplicative constant applied to the ACIS-S3 spectra $c = 0.85^{+0.43}_{-0.26}$ (consistent with unity) are evidence that the *Chandra* spectrum is consistent with the *XMM*-EPIC spectra, within the uncertainty.

(1.2 counts out of 48 in the source extraction region) can be neglected, as required by Cash-statistic. For comparison purposes with the *XMM* spectral fitting, the chosen model here is nsatmos alone (with fixed wabs absorption, distance and mass as before), which assumes that the PL component observed in the *XMM* spectrum is not intrinsic to the candidate qLMXB, i.e., that in the *XMM* spectrum, the PL tail is due to contaminating nearby sources. The best-fit value are $R_{\rm NS} = 6.6^{+3.2}_{-1.3}$ km ($M_{\rm NS} = 1.4\,M_\odot$) and $kT_{\rm eff} = 134^{+35}_{-39}$ eV, which are in remarkable agreement with the values obtained from the *XMM* observation. The 0.5–10 keV unabsorbed X-ray flux is $F_{\rm X} = 1.0\times10^{-13}\,{\rm erg\,cm^{-2}\,s^{-1}}$. These results are also listed in Table 3, for a convenient comparison with the *XMM* spectral fits.

4. DISCUSSION AND CONCLUSION

Using the *XMM* observation of NGC 6553, we have spectrally identified one candidate qLMXB in the GC. The best-fit nsatmos parameters found are $R_{\rm NS} = 6.3^{+2.3}_{-0.8}$ km (for $M_{\rm NS} = 1.4\,M_\odot$) and $kT_{\rm eff} = 136^{+21}_{-34}$ eV,

and the best-fit PL photon index is $\Gamma = 2.1^{+0.5}_{-0.8}$. The low-S/N *Chandra* spectrum finds consistent best-fit values within the statistic permitted by the detected counts. The modest precision of the NS radius measurement obtained with these short exposures does not permit to place constraints on the dense matter EoS. Deeper *Chandra* exposures will provide the S/N necessary to confirm the classification and to produce useful uncertainty on the radius measurement for the determination of the dense matter EoS.

The number of candidates identified in NGC 6553 (only 1) is in agreement with that predicted from the relations $N_{\mathrm{qNS}} \sim 0.04 \times \Gamma_{\mathrm{GC}} + 0.2$ (Gendre et al. 2003) and $N = 0.993 \times \Gamma_{\mathrm{GC}} - 0.046$ (Heinke et al. 2003b), where the authors used different normalizations for Γ_{GC}; the encounter rate of the GC is defined by $\Gamma_{\mathrm{GC}} \propto \rho_0^{1.5} r_{\mathrm{c}}^2$ (Verbunt 2003). In this last equation, ρ_0 is the central luminosity density (in $L_{\odot}\,\mathrm{pc}^{-3}$) and r_{c} is the core radius (in pc, not angular distance). Quantitatively, using the same respective normalizations, the number of expected qLMXBs in NGC 6553, given $\rho_{0,\mathrm{NGC\ 6553}} = 3.84\ L_{\odot}\,\mathrm{pc}^{-3}$ (Harris 1996), are 0.43 and 0.34 using the two relations cited above, respectively. Assuming Poisson statistics, the probability of finding one qLMXB when 0.43 (0.34) are expected is 28% (24%). Therefore, our findings are not in disagreement with these two empirical predictions.

The total unabsorbed *XMM* flux of the candidate qLMXB, $F_{\mathrm{X}} = 1.5^{+4.3}_{-0.7} \times 10^{-13}\,\mathrm{erg\ cm^{-2}\ s^{-1}}$, includes a PL component with a $33^{+35}_{-22}\%$ contribution to the flux. If intrinsic to the source, this PL component has one of the strongest contribution to the total flux ever observed for a qLMXB in a GC (others are in NGC 6440 and 47Tuc, Heinke et al. 2003b, 2005, respectively). However, we have shown evidences for the presence of nearby contaminating sources. This is tentatively supported by a short archived *Chandra* observation, but the low-significance detection of the nearby sources does not confirm with certainty the existence of contamination. Only a longer *Chandra* observation would confirm the spectral classification of the bright core source and confirm the detection of the faint neighboring core sources.

The candidate qLMXB did not display X-ray variability on the time scale of the observation. Specifically, there was no evidence that the *XMM* integrated light curve is significantly different from a linear distribution of counts. Regarding the long time scale variability, there is no significant change of flux between the *XMM* and *Chandra* observations. We also searched for archived *ROSAT* observation, but no source was detected at the position of XMMU J180916−255425 on the PSPC survey, and no HRI observation at the center of the GC was performed.

To conclude, the candidate in the core of NGC 6553, with $L_{\mathrm{X,th}} = 4.2 \times 10^{32}\,\mathrm{erg\ s^{-1}}$ $(d = 6\,\mathrm{kpc})$, adds to the small list of known GC qLMXB. However, only a high enough S/N observation with *Chandra* will allow to confirm with certitude the spectral classification of the source, and will be able to provide constraints on the dense matter EoS.

REFERENCES

Arnaud, K. A. 1996, in Astronomical Society of the Pacific Conference Series, Vol. 101, Astronomical Data Analysis Software and Systems V, ed. G. H. Jacoby & J. Barnes, 17–+

Asai, K., Dotani, T., Hoshi, R., Tanaka, Y., Robinson, C. R., & Terada, K. 1998, PASJ, 50, 611

Asai, K., Dotani, T., Mitsuda, K., Hoshi, R., Vaughan, B., Tanaka, Y., & Inoue, H. 1996, PASJ, 48, 257

Bildsten, L., Salpeter, E. E., & Wasserman, I. 1992, ApJ, 384, 143

Bordas, P. et al. 2010, The Astronomer's Telegram, 2919, 1

Brown, E. F., Bildsten, L., & Rutledge, R. E. 1998, ApJ, 504, L95+

Cackett, E. M., Brown, E. F., Miller, J. M., & Wijnands, R. 2010, ApJ, 720, 1325

Cackett, E. M. et al. 2005, ApJ, 620, 922

Campana, S. et al. 2004, ApJ, 614, L49

Campana, S. & Stella, L. 2000, ApJ, 541, 849

Campana, S., Stella, L., Mereghetti, S., Colpi, M., Tavani, M., Ricci, D., Fiume, D. D., & Belloni, T. 1998, ApJ, 499, L65+

Cash, W. 1979, ApJ, 228, 939

Degenaar, N. & Wijnands, R. 2011, MNRAS, 412, L68

Dempsey, R. C., Linsky, J. L., Schmitt, J. H. M. M., & Fleming, T. A. 1993, ApJ, 413, 333

Dickey, J. M. & Lockman, F. J. 1990, ARA&A, 28, 215

Fridriksson, J. K. et al. 2010, ApJ, 714, 270

Fruscione, A. et al. 2006, in Society of Photo-Optical Instrumentation Engineers (SPIE) Conference Series, Vol. 6270, Society of Photo-Optical Instrumentation Engineers (SPIE) Conference Series, 62701V

Garmire, G. P., Bautz, M. W., Ford, P. G., Nousek, J. A., & Ricker, Jr., G. R. 2003, in Society of Photo-Optical Instrumentation Engineers (SPIE) Conference Series, Vol. 4851, Society of Photo-Optical Instrumentation Engineers (SPIE) Conference Series, ed. J. E. Truemper & H. D. Tananbaum, 28–44

Gendre, B., Barret, D., & Webb, N. A. 2003, A&A, 403, L11

Graessle, D. E., Evans, I. N., Glotfelty, K., He, X. H., Evans, J. D., Rots, A. H., Fabbiano, G., & Brissenden, R. J. 2007, Chandra News, 14, 33

Grindlay, J. E., Heinke, C., Edmonds, P. D., & Murray, S. S. 2001, Science, 292, 2290

Guainizzi, M. 2008

Guillot, S., Rutledge, R. E., Bildsten, L., Brown, E. F., Pavlov, G. G., & Zavlin, V. E. 2009a, MNRAS, 392, 665

Guillot, S., Rutledge, R. E., Brown, E. F., Pavlov, G. G., & Zavlin, V. E. 2009b, ApJ, 699, 1418

Gupta, S., Brown, E. F., Schatz, H., Möller, P., & Kratz, K.-L. 2007, ApJ, 662, 1188

Haensel, P. & Zdunik, J. L. 2008, A&A, 480, 459

Harris, W. E. 1996, AJ, 112, 1487

Heinke, C. O., Grindlay, J. E., & Edmonds, P. D. 2005, ApJ, 622, 556

Heinke, C. O., Grindlay, J. E., Lloyd, D. A., & Edmonds, P. D. 2003a, ApJ, 588, 452

Heinke, C. O., Grindlay, J. E., Lugger, P. M., Cohn, H. N., Edmonds, P. D., Lloyd, D. A., & Cool, A. M. 2003b, ApJ, 598, 501

Heinke, C. O., Rybicki, G. B., Narayan, R., & Grindlay, J. E. 2006a, ApJ, 644, 1090

Heinke, C. O., Wijnands, R., Cohn, H. N., Lugger, P. M., Grindlay, J. E., Pooley, D., & Lewin, W. H. G. 2006b, ApJ, 651, 1098

Høg, E. et al. 2000, A&A, 355, L27

Høg, E., Kuzmin, A., Bastian, U., Fabricius, C., Kuimov, K., Lindegren, L., Makarov, V. V., & Roeser, S. 1998, A&A, 335, L65

Houk, N. & Smith-Moore, M. 1988, Michigan Catalogue of Two-dimensional Spectral Types for the HD Stars. Volume 4, Declinations -26°.0 to -12°.0., ed. Houk, N. & Smith-Moore, M.

Hut, P. et al. 1992, PASP, 104, 981

McClintock, J. E., Narayan, R., & Rybicki, G. B. 2004, ApJ, 615, 402

Ortolani, S., Renzini, A., Gilmozzi, R., Marconi, G., Barbuy, B., Bica, E., & Rich, R. M. 1995, Nature, 377, 701

Pooley, D., Homan, J., Heinke, C., Linares, M., Altamirano, D., & Lewin, W. 2010, The Astronomer's Telegram, 2974, 1

Predehl, P. & Schmitt, J. H. M. M. 1995, A&A, 293, 889

Riaz, B., Gizis, J. E., & Harvin, J. 2006, AJ, 132, 866

Rutledge, R. E., Bildsten, L., Brown, E. F., Pavlov, G. G., & Zavlin, V. E. 1999, ApJ, 514, 945

— 2001a, ApJ, 559, 1054

— 2001b, ApJ, 551, 921

— 2002, ApJ, 577, 346

Strüder, L. et al. 2001, A&A, 365, L18

Valenti, E., Ferraro, F. R., & Origlia, L. 2007, AJ, 133, 1287

van Paradijs, J., Verbunt, F., Shafer, R. A., & Arnaud, K. A. 1987, A&A, 182, 47

Verbunt, F. 2003, in Astronomical Society of the Pacific Conference Series, Vol. 296, New Horizons in Globular Cluster Astronomy, ed. G. Piotto, G. Meylan, S. G. Djorgovski, & M. Riello, 245—+

Voges, W. et al. 1999, A&A, 349, 389

Watson, M. G. et al. 2009, A&A, 493, 339

Webb, N. A. & Barret, D. 2007, ApJ, 671, 727

Zacharias, N., Monet, D. G., Levine, S. E., Urban, S. E., Gaume, R., & Wycoff, G. L. 2005, VizieR Online Data Catalog, 1297, 0

Zavlin, V. E., Pavlov, G. G., & Shibanov, Y. A. 1996, A&A, 315, 141